ELSEVIER

Journal of Alloys and Compounds 292 (1999) 134–147

Journal of ALLOYS AND COMPOUNDS

SANS measurements of deuteride (hydride) formation in single crystal Pd

Brent J. Heuser[a,*], John S. King[b], W.C. Chen[a]

[a]*University of Illinois, Department of Nuclear Engineering, Urbana, IL 61801, USA*
[b]*University of Michigan, Department of Nuclear Engineering, Ann Arbor, MI 48109, USA*

Received 8 February 1999; received in revised form 10 May 1999; accepted 10 May 1999

Abstract

In situ small-angle neutron scattering (SANS) measurements of deuteride precipitation in well-annealed, undeformed single crystal Pd have been performed at room temperature to observe the morphology of the precipitate as the deuterium fraction was increased over a range of 0.005 to 0.097 [D]/[Pd]. Supporting measurements were made of the room temperature deuterium solubility isotherm in the single crystal material and of the progressive lattice mosaic broadening by gamma-ray diffraction analysis. The use of single crystal material eliminated the effect of grain boundaries on the precipitation process and allowed the orientation of the deuteride precipitates relative to the host Pd lattice to be established. The SANS data for deuterium loading beyond the solid solution phase are dominated by a $d\Sigma/d\Omega \sim Q^{-2}$ scattering response well fit by a model cross section of small plate-like precipitates with a thickness of 25–30 Å. This response showed little indication of a preferred habit plane and the plate thickness was independent of the total deuterium loading. The volume fraction of these small plates grew uniformly with increased deuterium loading, but was surprisingly small, reaching only 8×10^{-5} at 0.060 [D]/[Pd]. This means that almost all of the deuterium resides in some other precipitate structure. The SANS data in the lowest Q region showed a second, anisotropic scattering component that can be interpreted as the Porod tail from plate-like particles of grossly larger dimensions. These plates favor a $(001)_\alpha$ habit plane, normal to the elastically soft $[001]_\alpha$ direction. Post-measurement visual inspection of the sample surfaces showed the presence of an oriented, quasi-periodic one-dimensional array of plates with thicknesses of approximately 0.1 to 0.2 mm and with an orientation in agreement with the anisotropy of the SANS data. We conclude that most of the deuteride phase precipitates in these large structures.

Keywords: Deuterium; Palladium; Single crystal; Hydride; Morphology

1. Introduction

The behavior of hydrogen in bulk metals and alloys has been investigated for many decades. Work in this area continues to be driven by the deleterious effects of hydrogen embrittlement in many engineering applications, by the search for more efficient hydrogen storage media, and by fundamental interests in diffusion, defect trapping, and phase transformation phenomena [1]. An understanding of conditions governing the formation of hydrogen-rich phases is often critical in applications involving metals exposed to hydrogen containing environments. A significant portion of past experimental work in this area has relied upon transmission electron microscopy analysis of the hydride structure, morphology and transformation-induced lattice damage [2–5].

One pertinent issue that remains largely unexplored, at least experimentally, is the true nature of the hydride phase transformation process; whether coherent nucleation occurs, and if so, is coherency lost during growth. In general, coherent nucleation is favored because the free energy barrier height for small coherent particles is much less than that for semi-coherent or incoherent particles of the same size [6]. This general statement has been placed on a firm theoretical foundation by Cahn and Larché [7]. These authors demonstrated that the elastic energy associated with coherent nucleation invalidates the Gibbs phase rule governing incoherent phase separation, and show, at least theoretically, that incoherent phase separation can only occur in the limit of vanishing coherent elastic energy (or vanishing transformation volume misfit). More recently, an explanation of the hysteresis phenomena that is specifically applicable to metal–hydrogen systems has been advanced by Schwarz and Khachaturyan [8]. Isothermal pressure hystereses common in metal–hydrogen systems, which are not explicitly treated by Cahn and Larché, are seen by Schwarz and Khachaturyan to be a direct consequence of the coherent elastic free energy term.

*Corresponding author.

0925-8388/99/$ – see front matter
PII: S0925-8388(99)00256-X

Palladium was used for much of the early experimental work in the study hydride formation in metals and is now recognized as test-bed material. Interestingly, the large body of experimental observations of the Pd–H phase transformations and associated pressure hysteresis appear to contradict the above arguments. It is well known that both the $\alpha \rightarrow \alpha'$ transformation and $\alpha' \rightarrow \alpha$ reversion generate high dislocation densities in Pd, as has been observed in numerous solubility measurements [9,10] and with transmission electron microscopy (TEM) [5]. Although not conclusive, thermodynamic models that relate the difference in chemical potential between the two pressure branches of the hysteresis to dislocation formation enthalpy give realistic results [11,12]. Based on these observations, the hydride phase transformation in Pd is thought to proceed by the growth of semi-coherent or incoherent particles, with associated dislocation generation.

Still, the existing experimental evidence is incomplete and questions concerning the phase transformation process remain unanswered. Solubility isotherm measurements yield limited information, offering a characterization of the pressure hysteresis without providing information about the particle morphology. This information is important, however; volume-misfit stresses will dictate the equilibrium particle shape and orientation relative to the host lattice at the onset of nucleation. Particle shape and coherency can be determined with TEM [2,5]. However, it is difficult, if not impossible, to perform TEM analysis as a function of known, controlled hydrogen concentration. Furthermore, all TEM analysis is performed within a few thousand Angstroms of two free surfaces. The strain energy associated with lattice defects and free surfaces can alter the precipitation process. Thus, the true nature of the hydride transformation is difficult to determine with TEM.

Small-angle neutron scattering (SANS) can provide hydride particle shape information, particle orientation relative to the single crystal lattice for anisometric particles, and can serve as a sensitive monitor of early precipitation [13]. The ability of SANS to yield deuteride precipitation information over a bulk scale is demonstrated by initial experiments with deuterium-loaded, single crystal Pd presented here.

2. Experimental

Two well-annealed, single crystal Pd samples, SC17 and SC18, with altogether five deuterium atomic fractions, 0.017, 0.031, 0.058, 0.060, and 0.097 [D]/[Pd], as well as a zero fraction background, were characterized with SANS. These samples were prepared from a 99.999% pure single crystal Pd ingot grown by Metal Crystals and Oxides of Cambridge, UK. The cylindrical ingot was grown by the Czochralski method with a [110] axis, 10 cm in length and approximately 1.0 cm in diameter. Wafers were cut from the as-grown ingot using a low speed diamond saw and mechanically polished to remove surface irregularities. 0.03 μm levitated alumina was used in the final polishing step. Both samples consisted of two wafers. This increased the surface-to-volume ratio, thereby facilitating deuterium loading. Each wafer was approximately 1 cm diameter, 0.16 cm thick and weighed 1.5 g (for a total sample mass of 3 g). The crystallographic orientation of each wafer was matched as the sample was loaded into the measurement cell. The orientation of the wafers was confirmed by neutron diffraction.

The two samples were incrementally advanced, with one sample placed on the spectrometer while the other was loading to the next (higher) deuterium fraction. The following deuterium loading sequences were followed for the two samples: SC17; $0.0 \rightarrow 0.017 \rightarrow 0.060 \rightarrow 0.097$ [D]/[Pd], SC18; $0 \rightarrow 0.031 \rightarrow 0.058$ [D]/[Pd]. The SC17 and SC18 labels will be omitted and all references to the SANS measurements will use the deuterium fraction only. In addition, a third well-annealed, single crystal sample from the same ingot loaded to 0.005 [D]/[Pd] (well below the solubility limit of deuterium in the α phase of Pd) was previously characterized with SANS [14]. These results are reported here as well. Deuterium is used for the SANS measurements because the coherent scattering cross section of the deuteron is over three times larger than that of the proton, while the incoherent, or background, scattering cross section is a factor of 40 lower. The two samples were each held in identical ultra high vacuum stainless steel gas cells. Each cell was equipped with two sapphire windows to reduce empty-cell neutron scattering. Deuterium loading was accomplished by exposure to deuterium gas at room temperature. Each sample was pre-annealed in the gas cells under vacuum at 150°C for approximately 2 h before the first exposure to deuterium gas. As discussed below, large over-pressures (gas-exposure pressures well above the two-phase region plateau pressure) were required to increase the deuterium concentration above 0.017 [D]/[Pd]. Deuterium fractions were determined by total pressure change in the combined volume of the cell and vacuum manifold used for D_2 exposure. The total volume of the manifold and sample cell was 1172 cm^3. The D_2 gas pressure was reduced to a value near plateau pressure after loading. The sample cell was then isolated from the loading manifold, reducing the gas reservoir volume to less than 10 cm^3. This small volume prevented significant concentration changes in the samples during the SANS measurements.

The SANS measurements were performed at the National Institute of Standards and Technology (NIST) Center for Neutron Research using the 30 m NSF (NG3) instrument [15]. The sealed gas cells were rigidly mounted in the standard spectrometer sample box, which was evacuated and back-filled with helium. All samples were measured at room temperature with the instrument in two resolution configurations. To probe the high wave-vector transfer region, $0.03 \leq Q \leq 0.4$ $Å^{-1}$, (Q is given by $Q = (4\pi/\lambda) \sin$

θ, where λ is the neutron wavelength and θ is half the scattering angle), the instrument was configured as follows: source-to-sample distance of 382 cm (eight guides inserted), sample-to-detector distance of 160 cm, beam-stop diameter of 5.08 cm, sample aperture diameter of 0.70 cm, source aperture diameter of 5 cm, 20 cm horizontal detector off-set, and the neutron wavelength of 6.0 ± 0.9 Å ($\pm$FWHM). This setting is referred to as the high-Q configuration below. The low-Q configuration, $0.007 \leq Q \leq 0.1$ A^{-1}, was obtained by changing the source-to-sample distance to 832 cm (five guides inserted) and the sample-to-detector distance to 600 cm while holding all other instrument setting parameters fixed. Absolute cross section calibration was performed in the high-Q configuration using the incoherent scattering from 0.1 cm of water. The low-Q data were then scaled to the high-Q cross sections over a common data range of approximately $0.04 \leq Q \leq 0.08$ A^{-1}. The integrated counting rates over the entire 65×65 cm area detector are given in Table 1.

A fourth undeformed sample (0.3 cm, 3 g) from the same single crystal ingot was used to determine the room temperature deuterium solubility behavior in the single crystal material. The solubility measurement was performed at the University of Illinois in a stainless steel gas system. Deuterium atomic fractions were determined by recording the D_2 gas pressure decrease during absorption (or pressure increase during desorption) in the closed volume (1125 cm^3) of the vacuum system. The isotherm measurement was terminated at 0.33 [D]/[Pd]. The desorption branch plateau pressure was then recorded by gas evolution to 0.28 [D]/[Pd].

Evidence of lattice distortion induced by the $\alpha \rightarrow \alpha'$ phase transformation in the single crystal Pd matrix was obtained from gamma-ray diffraction analysis. These measurements were performed using the Missouri University Gamma-ray Spectrometer instrument at the University of Missouri Research Reactor Facility. An activated gold source (0.412 MeV gamma-ray energy corresponding to a 0.030 Å wavelength) was used to ensure bulk penetration in Pd. The angular resolution of the collimation system was approximately 12 min of arc FWHM.

3. Results

3.1. Room-temperature isothermal solubility

The deuterium solubility behavior of single crystal material is helpful in determining the location of the each SANS measurement on the room temperature isotherm. However, the room temperature isothermal solubility behavior of hydrogen or deuterium has never been measured in well-annealed single crystal Pd beyond the α phase [16]. Grain boundaries act as trap site for interstitial solutes [17]. This trapping interaction can alter the solid solution solubility behavior, possibly promoting heterogeneous nucleation. It is therefore informative to compare the single crystal solubility measurement to the known polycrystalline solubility behavior. The room temperature deuterium solubility isotherm in the single crystal Pd material is presented in Fig. 1. The isotherm was tracked to 0.33 [D]/[Pd] during absorption, followed by a desorption measurement to 0.28 [D]/[Pd]. The deuterium isotherm in polycrystalline Pd at 298°C from Ref. [22] is shown for comparison.

The D_2 gas pressure was observed to change exponentially with time during the solubility measurements. The characteristic time constants of the exponential pressure change are shown in Fig. 2. The initial time constant during absorption in the solid solution region is consistent with regular lattice diffusion. The absorption behavior within the two-phase region is dramatically slower, with the time constant falling by over an order of magnitude. In fact, the kinetics were so slow that the measurement at 0.254 [D]/[Pd] required 48 days to reach 94% completion. After an initial transition period, the decomposition kinetics within the two-phase region (the 0.28 [D]/[Pd] point) are similar to those governing phase formation.

3.2. Small-angle neutron scattering

The absolute macroscopic, differential scattering cross section, $d\Sigma/d\Omega$, for all deuterium fractions measured in the high and low Q configurations are shown in Figs. 3 and

Table 1
Integrated counting rates over the detector

Sample	Low-Q configuration (s^{-1})	High-Q configuration (s^{-1})
Beam-blocked background	3.0	11.2
Open beam	13.3	101
Zero conc.	10.9	107
0.017 [D]/[Pd]	–	121
0.031 [D]/[Pd]	12.3	126
0.058 [D]/[Pd]	15.3	–
0.060 [D]/[Pd]	16.0	145
0.097 [D]/[Pd]	19.3	–

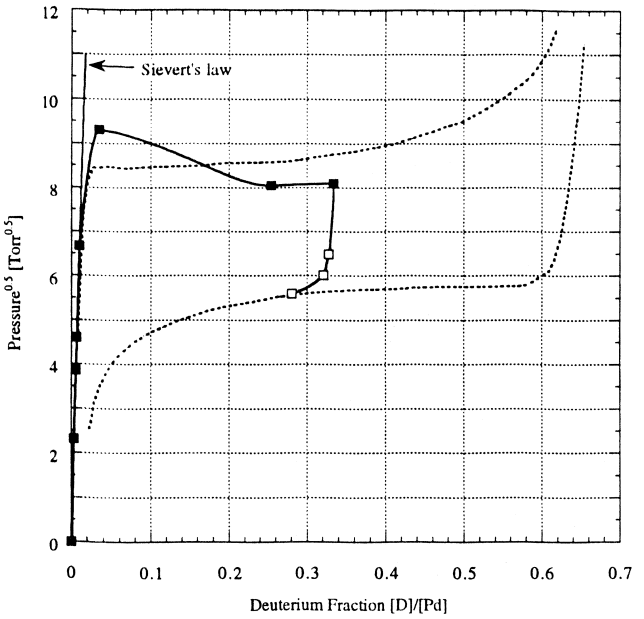

Fig. 1. Deuterium solubility isotherms in single crystal Pd at 300 K (this work, solid line) and polycrystalline Pd at 298 K (from Ref. [22], dotted line).

4, respectively. These data are radial averages over all azimuthal angles recorded by the detector. Only two fractions, 0.031 and 0.060 [D]/[Pd], were measured in both instrument configurations.

The net cross sections from the high-Q configuration, determined by subtracting the zero fraction reference measurement from the non-zero measurements, are shown in ln–ln format in Fig. 5. These data are fit with the single particle form factor for a plate plus an incoherent scattering term [19],

$$\frac{d\Sigma}{d\Omega}(Q) = 2\pi f\, T\, \frac{\Delta\rho^2}{Q^2} \exp\left(\frac{-Q^2T^2}{12}\right) + \frac{d\Sigma}{d\Omega_i} \cong 2\pi f\, T\, \frac{\Delta\rho^2}{Q^2} + \frac{d\Sigma}{d\Omega_i}, \quad (1)$$

where T is the plate thickness, f is the volume fraction of deuteride particles resulting in the Q^{-2} response, $\Delta\rho$ is the scattering length density contrast between the deuteride phase and the Pd matrix ($\Delta\rho = 2.33\times10^{10}$ cm^{-2}), and $d\Sigma/d\Omega_i$ is the incoherent scattering cross section from deuterium in the Pd lattice (incoherent scattering from Pd is eliminated in the net cross section subtraction). The right-hand side is written under the assumption that $QT \leq 1$, so that the Guinier-type exponential modifier can be dropped, resulting in a pure Q^{-2} law plus the incoherent term.

Although omitted in the fitting procedure, the high-Q data are sensitive to the effect of the exponential correction term given in Eq. (1). The magnitude of T can be determined by first subtracting the incoherent deuterium cross section (determined by the fit of Eq. (1)) from the net data, then plotting ln[net $d\Sigma/d\Omega\times Q^2$] vs. Q^2. This analysis is shown in Fig. 6. The solid lines are best fits to the linear portion for each deuterium fraction and give $T^2/12$ directly. The values of T are listed in Table 2. Even with the low statistics for the 0.017 [D]/[Pd] case, a very consistent value for T between 25 and 30 Å is obtained, independent of the deuterium loading.

The volume fraction of the deuteride phase bound in the small plates, f, can also be determined from the fit of Eq. (1) to the data once the plate thickness is known. The values shown in Table 2 were calculated using a plate thickness of 25 Å. The volume fraction of the small plate component is clearly a minute fraction of the total α' phase as determined from the lever rule. It is apparent from this analysis that the vast majority of the precipitated α' phase is in the form of large deuteride plates. The exception is the 0.017 [D]/[Pd] deuterium fraction in which the total α' phase volume fraction cannot be determined from the lever rule.

Radial average, net cross sections from the low-Q configuration data are presented in Fig. 7, again in ln–ln format. This figure includes the 0.097 [D]/[Pd] data not measured with the high-Q configuration and the net 0.005 [D]/[Pd] measurement. The 0.005 [D]/[Pd] data set clearly demonstrates that solid-solution levels of deuterium in the well-annealed single crystal Pd do not result in a significant SANS response. Eq. (1) does not take into account the scattering response of large deuteride particles

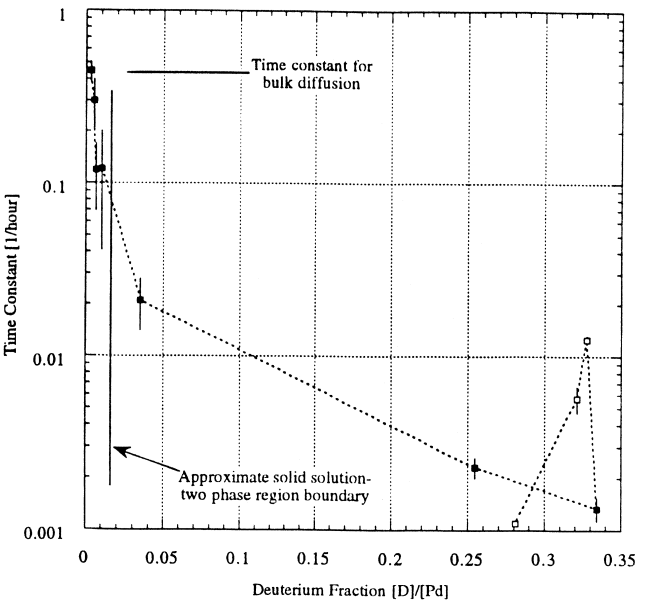

Fig. 2. Exponential time constants vs. deuterium fraction for the D_2 gas pressure variation observed during solubility measurements of the single crystal Pd material.

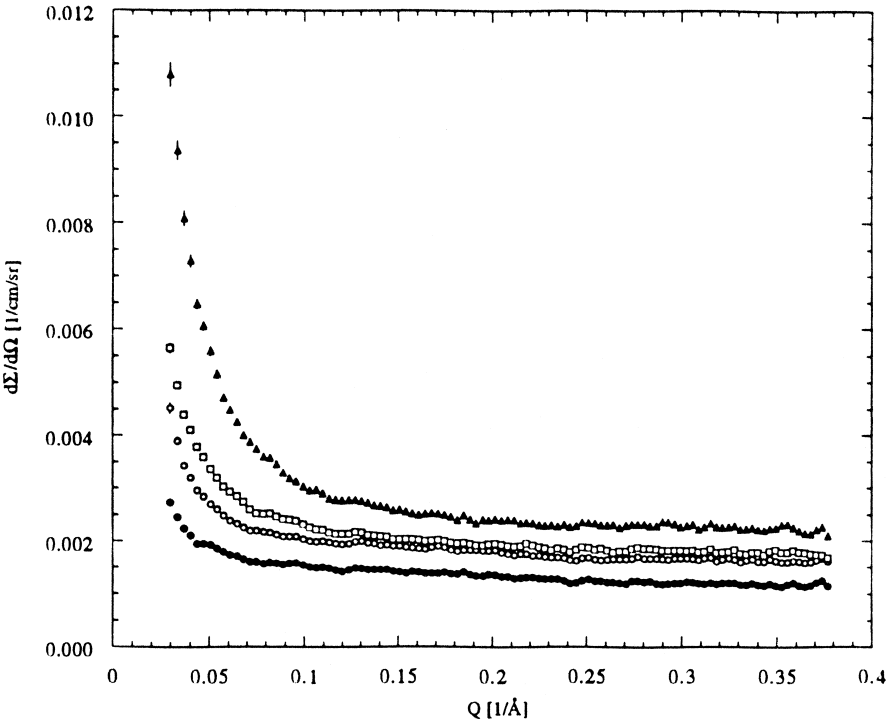

Fig. 3. Radial average macroscopic differential scattering cross sections, $d\Sigma/d\Omega$, vs. wavevector transfer, Q, measured in the high-Q configuration for the zero fraction (solid circles), 0.017 [D]/[Pd] (open circles), 0.031 [D]/[Pd] (open boxes), and 0.060 [D]/[Pd] (solid triangles).

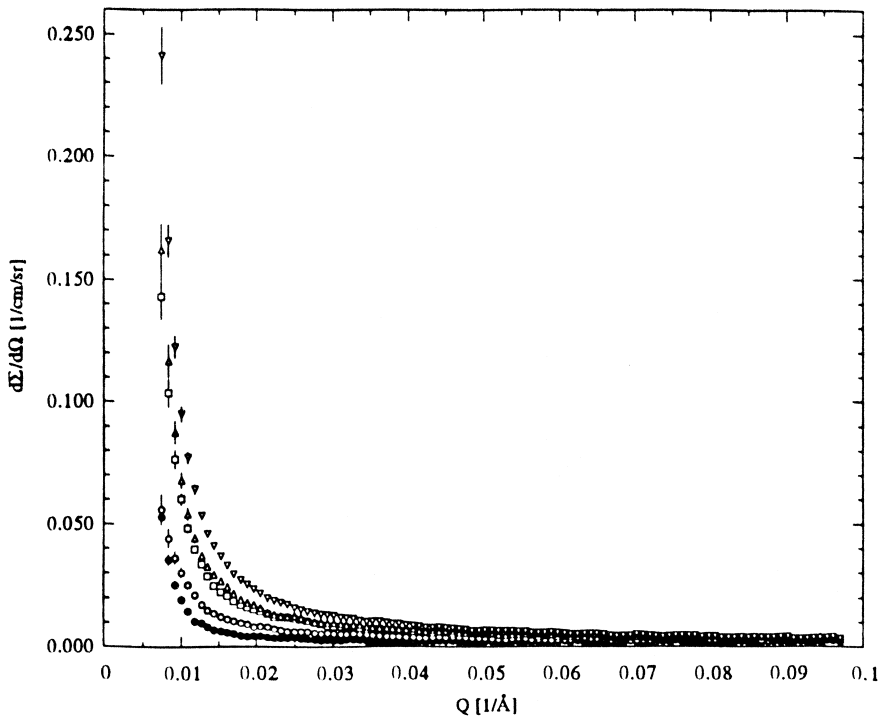

Fig. 4. Radial average macroscopic differential scattering cross sections, $d\Sigma/d\Omega$, vs. wavevector transfer, Q, measured in the low-Q configuration for the zero fraction (solid circles), 0.031 [D]/[Pd] (open circles), 0.058 [D]/[Pd] (open boxes), 0.060 [D]/[Pd] (open triangles), and 0.097 [D]/[Pd] (inverted open triangles).

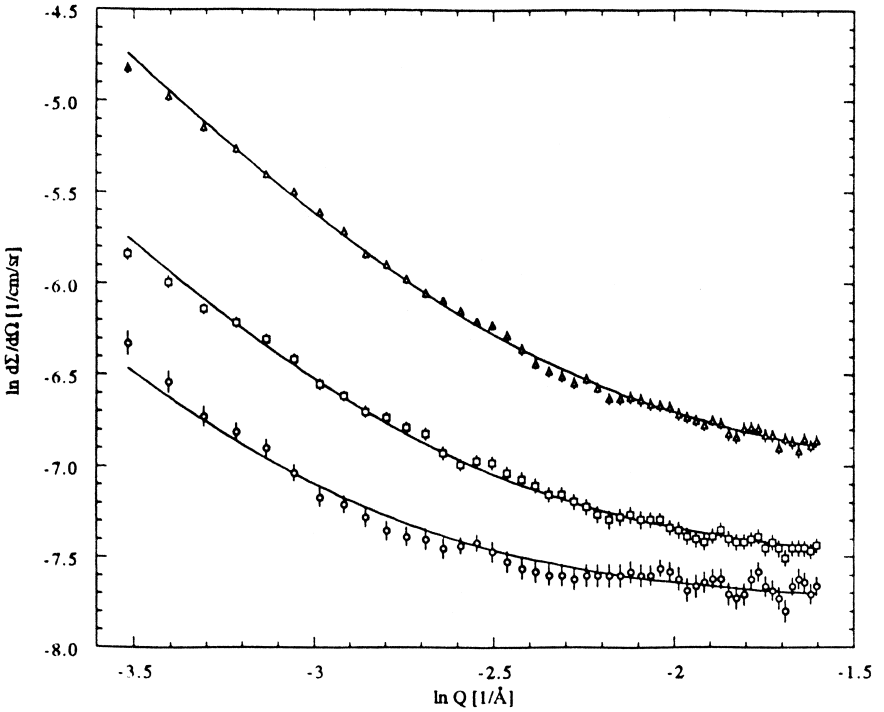

Fig. 5. Net SANS cross sections for 0.017 [D]/[Pd] (open circles), 0.031 [D]/[Pd] (open boxes), and 0.060 [D]/[Pd] (open triangles) in the high-Q configuration determined from a subtraction of the zero-fraction measurement. Solid lines are best fits of Eq. (1) to the net data. Q^{-2} scattering amplitudes from these fits are listed in Table 2.

which exhibit Porod behavior at the lowest limit of the low-Q configuration. The data in Fig. 7 (except for the 0.005 [D]/[Pd] measurement) are fit with the single particle form factor for plate geometry given in Eq. (1) plus the Porod law given by [24],

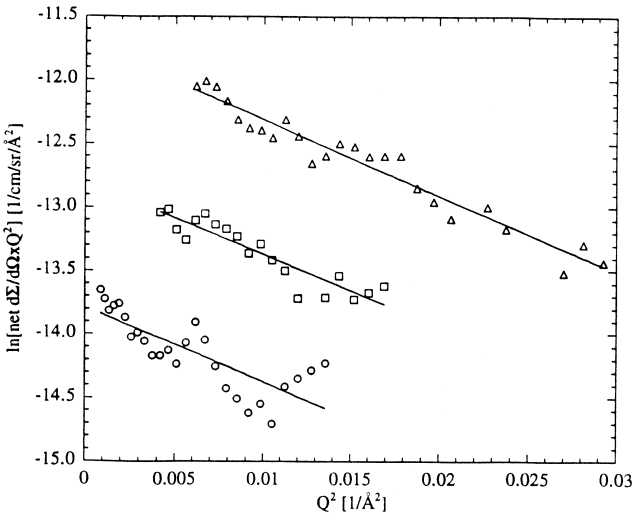

Fig. 6. ln[net $d\Sigma/d\Omega \times Q^2$] vs. Q^2 (after subtraction of the deuterium incoherent scattering term) for 0.017 [D]/[Pd] (open circles), 0.031 [D]/[Pd] (open boxes), and 0.060 [D]/[Pd] (open triangles). Solid lines are fits over the linear portion of the data and give the average thickness of the deuteride plates causing the Q^{-2} scattering shown in Fig. 5 and discussed in the text. The reduced quality of the data at the lowest deuterium fraction is due to the very small Q^{-2} scattering amplitude.

$$\frac{d\Sigma}{d\Omega}(Q) = \frac{4\pi\Delta\rho^2}{Q^4}\frac{S}{V}, \tag{2}$$

where S is the total interfacial surface area and V is the irradiated sample volume. This equation represents an average over all scattering object orientations [20] and is only appropriate for $QT >> 1$. The Porod response can exhibit noticeable anisotropy for oriented, highly anisometric particles, however. Anisotropy in the scattering response is presented in the next section. The Q^{-2} and Q^{-4} prefactor constants from Eqs. (1) and (2) are grouped together as ''amplitudes'' in Table 2.

3.3. Scattering anisotropy

Anisotropy in the SANS responses presented below is attributed to preferential alignment of anisometric, plate-like deuteride particles along specific directions in the Pd host lattice. In general, scattering from plate-like particles is expected to be peaked about an axis perpendicular to the face normal of the plate [13]. This is a direct consequence of the inverse relationship between particle dimension and scattering angle or Q. The small-angle scattering response is compressed into a small angular or Q range about $Q=0$ along in-plane directions of the plate. The resultant scattering then becomes peaked about the plate normal direction. On the other hand, isometric particles or a random arrangement of anisometric particles cannot result in an

Table 2
Fitting parameters from measured SANS cross sections

Sample [D]/[Pd]	Volume fraction of α′ phase from lever rule[a]	Q^{-4} amplitude ($x10^{-9}$ $cm^{-1}Å^{-4}sr^{-1}$)	Q^{-2} amplitude ($x10^{-5}$ $cm^{-1}Å^{-2}sr^{-1}$)	*T*, plate thickness (Å)	*f*, volume fraction of α′ phase in small plates
0.017	~0[b]	–	0.10±0.03	27±2	1×10^{-5}
0.031	0.027	0.08±0.02	0.24±0.03	25±1	3×10^{-5}
0.058	0.072	0.14±0.02	–	–	–
0.060	0.075	0.18±0.02	0.70±0.06	27±1	8×10^{-5}
0.097	0.14	0.28±0.02	–	–	–

[a] Lever rule calculation is based on the α–α′ two-phase region-boundaries at 0.015 and 0.60 [D]/[Pd].
[b] The lever rule cannot be accurately applied at the lowest deuterium fraction because the exact location of the low-concentration α–α′ boundary is uncertain. The volume fraction at 0.017 [D]/[Pd] is therefore listed as 0.

anisotropic scattering response. In the former case, scattering anisotropy cannot occur since the particle dimensions are approximately equal in all directions. In the latter case, the azimuthal dependency of the scattering would be smeared by the orientation averaging associated with the random arrangement.

The scattering anisotropy associated with the plate single particle form factor from the 0.017 and 0.060 [D]/[Pd] measurements is presented in Fig. 8, a plot of the Q^{-2} amplitude vs. detector azimuthal angle for 0.060 [D]/[Pd] (Fig. 8a) and 0.017 [D]/[Pd] (Fig. 8b). These data were obtained by averaging the scattering response over pie-shaped areas or sectors on the detector outward from the center. The 0.017 [D]/[Pd] data show a rough correlation between the deuteride plate orientation and the three high symmetry directions contained in the measured *Q*-plane. A change is evident as the deuterium fraction increases from 0.017 to 0.060 [D]/[Pd]. Comparing Fig. 8a and b, the increase in the Q^{-2} amplitude is disproportionately lower along the $[001]_\alpha$ direction. This is attributed to the growth of a subset of the plates on the $(00\bar{1})_\alpha$ habit plane to very large sizes. That is, the scattering from small plates at high *Q* is replaced by the scattering from large plates at low *Q*. This is supported by a comparison of the Q^{-2} and Q^{-4} scattering responses for the 0.060 [D]/[Pd] case shown in Fig. 9. The disproportionate increase of the

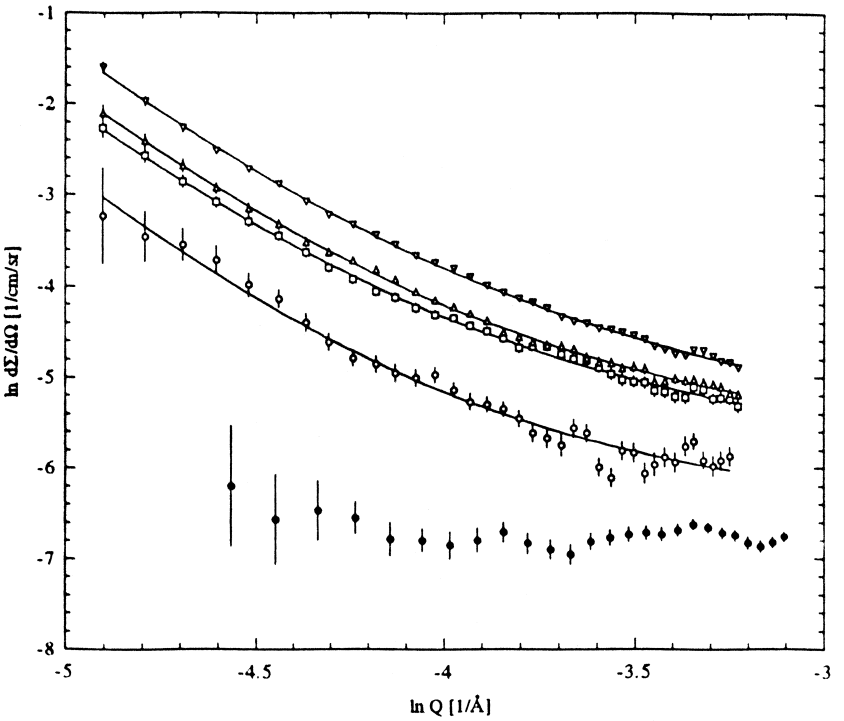

Fig. 7. Net SANS cross sections for 0.031 [D]/[Pd] (open circles), 0.058 [D]/[Pd] (open boxes), 0.060 [D]/[Pd] (open triangles), and 0.097 [D]/[Pd] (inverted open triangles) in the low-*Q* configuration determined from a subtraction of the zero fraction measurement. Solid lines are best fits of Eq. (2) combined with a Q^{-2} power law to the net data. Q^{-4} scattering amplitudes from these fits are listed in Table 2. The net SANS cross section from a well-annealed single crystal sample loaded to 0.005 [D]/[Pd] (solid circles) is shown for comparison. This deuterium fraction is well within the solid solution phase and demonstrates that no appreciable scattering occurs in the absence of deuteride precipitation.

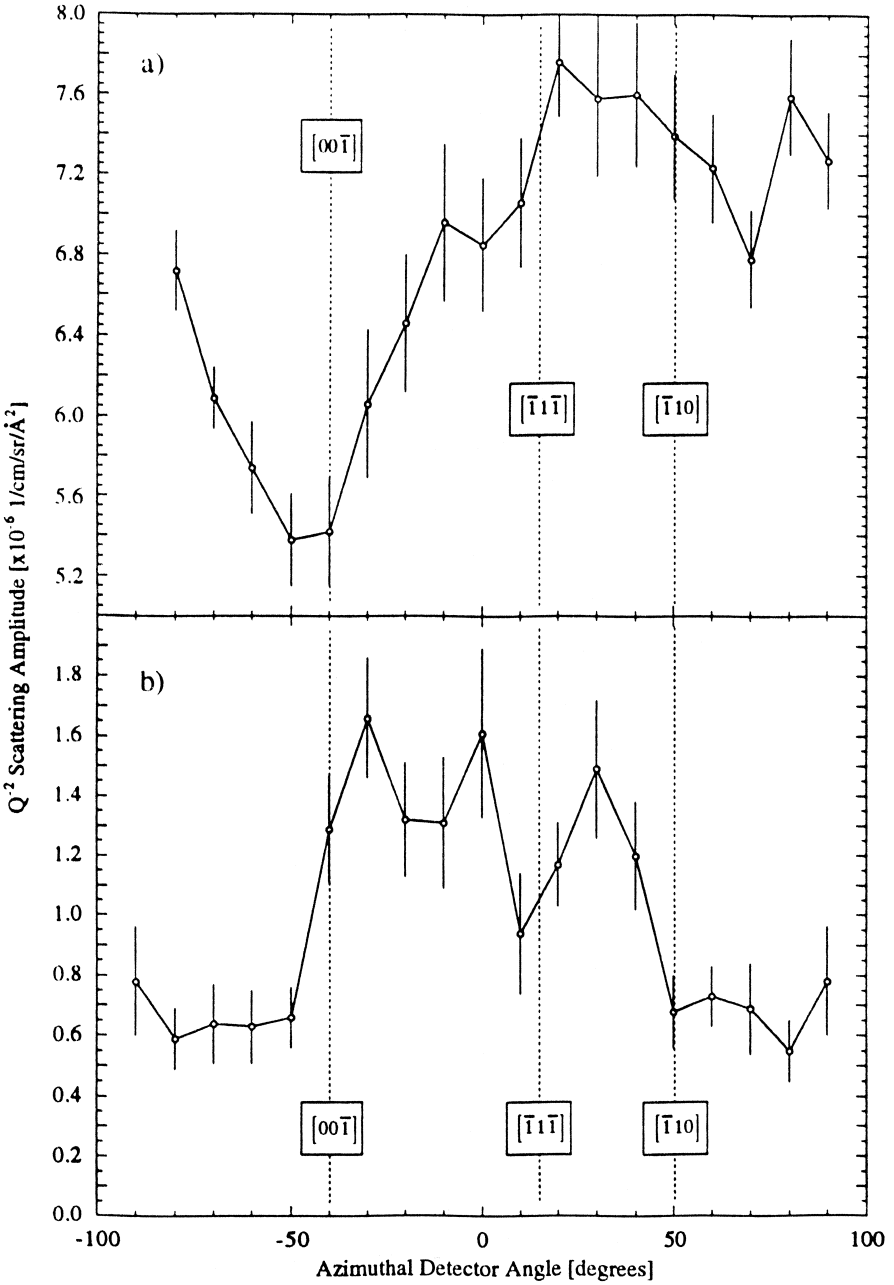

Fig. 8. Q^{-2} scattering amplitude vs. azimuthal detector angle for the 0.060 [D]/[Pd] (a) and 0.017 [D]/[Pd] (b) deuterium fraction SANS measurements. The three high symmetry Pd lattice directions contained in the measured Q plane are identified by the dotted vertical lines. The plotted amplitudes were determined by averaging the scattering response over pie-shaped areas on the detector $\pm 10°$ about each azimuthal or sector angle. This analysis establishes the correlation between the scattering anisotropy from the deuteride plates and the host lattice orientation, as discussed in the text.

Q amplitude corresponds reasonably well to an enhanced Porod response along the same $[001]_\alpha$ direction. Based on this analysis, we believe the Porod response observed at low Q is due to the precipitation of the very large ($T >$ 2000 Å) deuteride plates on the $(001)_\alpha$ habit plane.

Scattering anisotropy caused by mechanically polishing the sample surfaces was considered. The surface scratches left behind by mechanical polishing did not show a resolvable scattering anisotropy when sector averages were performed for the zero fraction reference.

3.4. Gamma-ray diffraction analysis

Additional insight into the hydride morphology may be inferred from the lattice distortion of the Pd host, characterized by gamma-ray diffraction rocking curve measurements, as the hydride fraction is increased. Scans of the (220) reflection, corresponding to the lattice planes perpendicular to the original ingot cylinder axis and parallel to the SANS sample surface, were performed for the reference sample and three additional samples with increasing

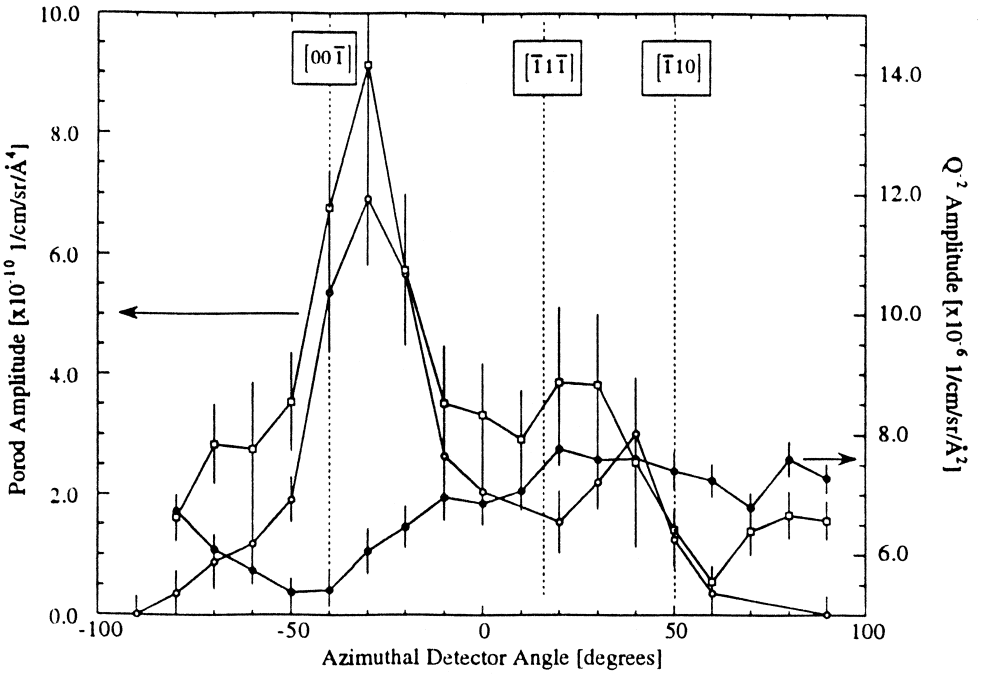

Fig. 9. Q^{-2} (solid circles) and Q^{-4} (open circles) scattering amplitudes vs. azimuthal detector angle for the 0.060 [D]/[Pd] deuterium fraction SANS measurement. The Q^{-4} scattering amplitude (open boxes) for 0.097 [D]/[Pd] is shown as well. The three high symmetry Pd lattice directions contained in the measured Q plane are identified by the dotted vertical lines. The plotted amplitudes were determined by averaging the scattering response over pie-shaped areas on the detector $\pm 10°$ about each azimuthal or sector angle. The suppressed Q^{-2} amplitude along $[00\bar{1}]_{\alpha}$ coincides with a sharp peak in the Porod response. This highly anisotropic Porod response is the result of large deuteride plates forming as the samples are driven into the two-phase region with large over-pressures.

levels of deuteride formation. These included the 0.058 [D]/[Pd] sample, the solubility-measurement sample, and an older sample, SC12, which had been fully hydride cycled (0.60 [D]/[Pd]) and used in a previous experiment [14]. In situ diffraction measurements were not possible and the samples were in varying states of gas desorption (SC12 was completely desorbed).

The (220) scans for the reference material and the 0.058 [D]/[Pd] sample are shown in Fig. 10, while scans for the 0.33 [D]/[Pd] and SC12 samples are shown in Fig. 11. Absolute intensities were not obtained during gamma-ray analysis. The data in Figs. 10 and 11 are normalized and fit with Gaussian profiles. The reference sample is well fit by a single Gaussian component, but for this narrow Bragg peak the measured width is essentially that of the instrumental resolution. Fits of the 0.058 [D]/[Pd] and SC12 samples require two Gaussian components, while the 0.33 [D]/[Pd] data is best fit with three Gaussian components. The dependence of the standard deviation of the Gaussian peaks vs. deuterium fraction is shown in Fig. 12 (the solid squares are for the narrow component and the open squares for the wide component). The narrow components for both the 0.058 and 0.33 [D]/[Pd] samples are the same, indicating that undamaged lattice remains. This is expected since these samples were not completely converted to the α' phase. SC12 was completely converted and the peak width demonstrates that significant lattice broadening has occurred.

Several in-plane reflections were characterized by gamma-ray diffraction but are not shown. All of these reflections exhibited a multi-peak structure, with several separate peaks spanning of a few degrees of arc. This structure is the result of low-angle tilt boundaries inducing slight angular misalignments between neighboring subcrystals. The difference between in-plane and the out-of-plane reflections may be due to the [110] growth axis of the ingot. The {220} family in an fcc lattice has lowest atomic area density of the three high symmetry planes and therefore represents an easy-growth axis, presumably with a corresponding low degree of disorder. Since the growth process is not perfect, some amount of disorder must be incorporated into the lattice and tilt boundaries form, presumably on planes orthogonal to the growth axis.

4. Discussion and analysis

4.1. Deuterium solubility in single crystal pd

The deuterium solubility behavior in single crystal Pd was within 10% of Sievert's law for the dilute concentration α phase. A noticeable deuterium supersaturation

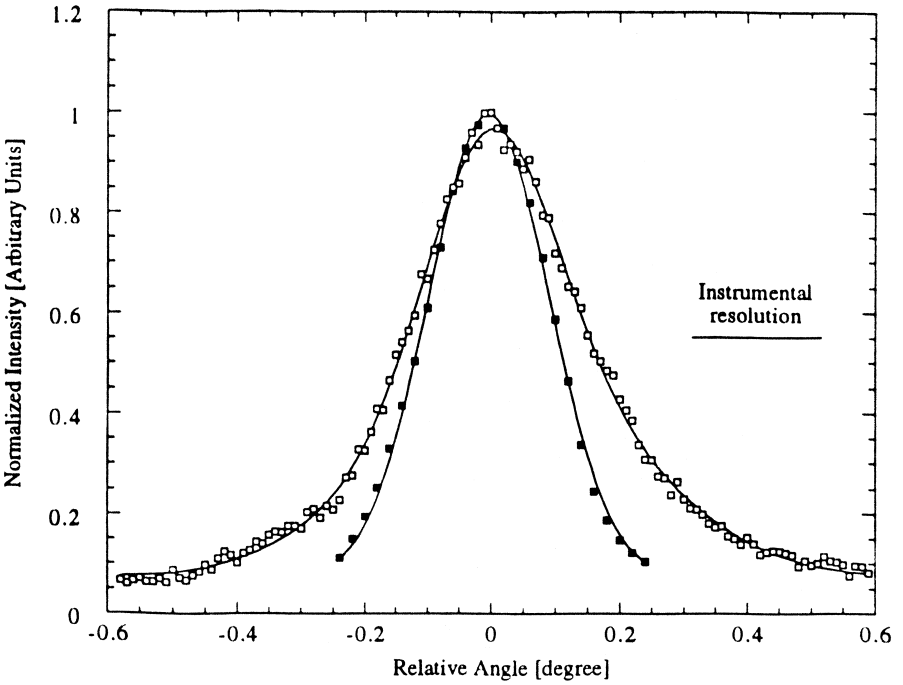

Fig. 10. Gamma-ray diffraction scan of the (220) out-of-plane reflection for well annealed, zero concentration single crystal Pd (solid boxes) and the 0.058 [D]/[Pd] sample (open boxes). The solid lines are Gaussian fits to the data. The measurement of the well annealed sample required a single component fit that was resolution limited. The measurement of the 0.058 [D]/[Pd] sample required two Gaussian components.

at the beginning of the single crystal two phase region is evident in Fig. 1. This feature is absent in the polycrystalline measurement of Flanagan et al. [18] reproduced in Fig. 1. The incremental height of this barrier can be estimated by the difference in chemical potential between the maximum pressure, p_1, and the plateau pressure, p_2,

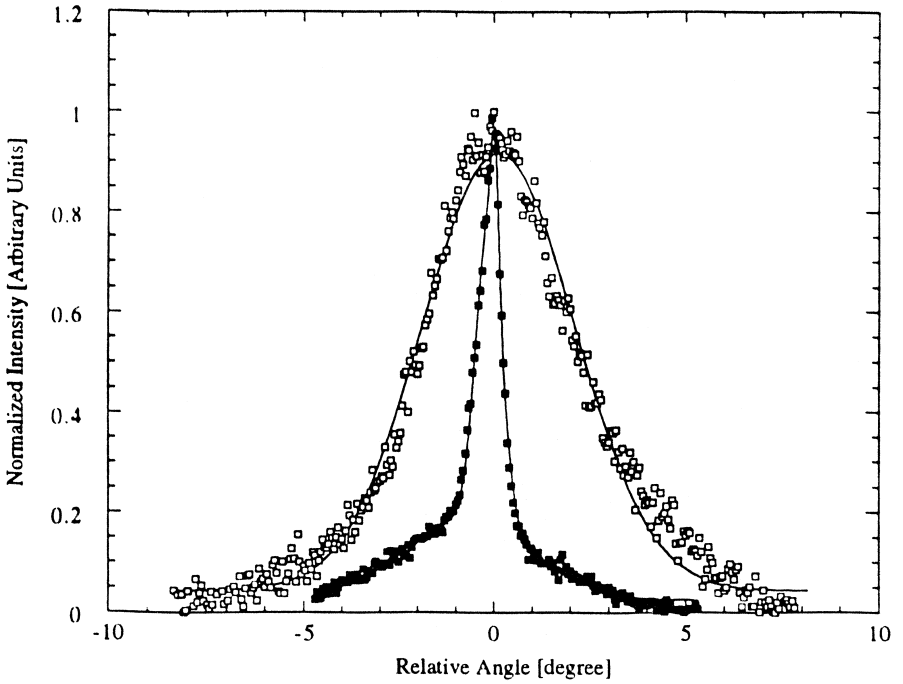

Fig. 11. Gamma-ray diffraction scan of the (220) out-of-plane reflection for the 0.33 [D]/[Pd] sample (solid boxes) and the 100% cycled sample (open boxes). The solid lines are Gaussian fits to the data. These measurements required three and two Gaussian component fits, respectively.

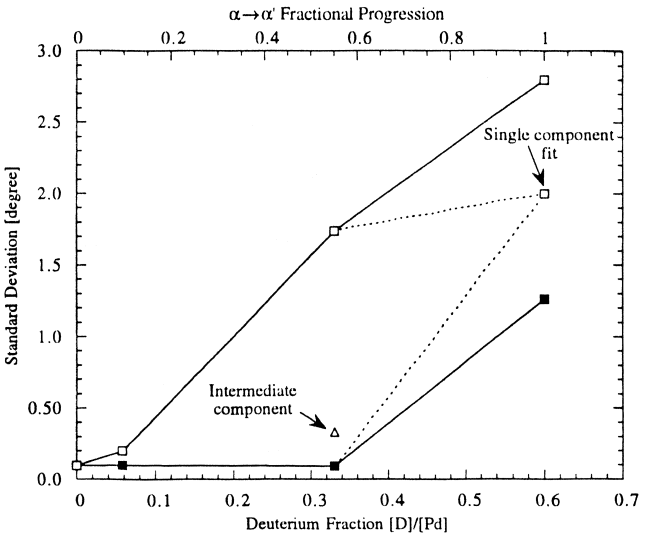

Fig. 12. A plot of the Gaussian-fit standard deviations for the (220) out-of-plane reflection as a function of deuterium fraction. The narrow component of the diffraction peak is preserved to very high deuterium fractions and only disappears after full conversion to α′. The third or intermediate component of the 0.33 [D]/[Pd] sample as well as a single component fit to the 100% cycled sample are identified in the figure.

$$\Delta\mu = \frac{1}{2} RT \ln\left(\frac{p_1}{p_2}\right), \tag{3}$$

resulting in a height of $\Delta\mu = 360$ J/mol D. The presence of an additional nucleation barrier may reflect a fundamental difference in the early stages of the phase transformation process in single crystal vs. polycrystalline Pd. One possible explanation is that the absence of the strain energy associated with grain boundary defects or second phase inclusions delays phase nucleation, resulting in the observed supersaturation and associated increase in chemical potential. This is also consistent with the notion that deuteride formation in single crystal Pd is occurring under homogeneous conditions. However, we do not believe this statement can be justified based on the existing solubility data. Although grain boundaries and second phase inclusions are not present in the single crystal material, small-angle or tilt boundaries exist, as do other, less organized clusters of dislocations. Homogeneous precipitation, even in a single crystal matrix, is seen as an idealized scenario, rare in practice. The added nucleation barrier in the single crystal material may still reflect heterogeneous nucleation, just not with complete stress relief that can occur with precipitation at grain boundaries.

An α phase supersaturation of $\Delta\mu \cong 70$ J/mol H at the α–α′ phase boundary has previously been observed for hydrogen absorption in well-annealed polycrystalline Pd [21]. However, this supersaturation was thought to be an artifact of the increased sluggishness of the transformation kinetics during the electrochemical solubility measurement, a conclusion supported the more recent gas-phase isothermal measurements by Flanagan et al. [18]. On the other hand, Wicke and Blaurock observed an α phase supersaturation and an α′ phase undersaturation during gas-phase solubility measurements, attributing the effect to a restraint on the initial nucleation process [22]. As shown in Fig. 2, a significant reduction in the gas-phase absorption kinetics was observed at the α–α′ boundary and within the two phase region. However, the solubility measurement corresponding to the supersaturation point in Fig. 1 (0.035 [D]/[Pd]) was recorded for a sufficiently long time (85 h or approximately two exponential-folding times) to characterize both the exponential time constant and the final solubility at equilibrium. We therefore consider the observed supersaturation to be a characteristic of the single crystal material (or Pd in general) during room temperature absorption and not an artifact of the measurement procedure.

Another feature of the solubility data is the lower single crystal absorption plateau pressure relative to the polycrystalline measurement of Flanagan et al. The difference in plateau pressures is small, though, approximately 5 Torr. The energy associated with the absorption–desorption hysteresis can also be analyzed with Eq. (3) for each case in Fig. 1. Although it is not clear that the single crystal desorption branch reached the plateau level, an estimate of $\Delta\mu = 930$ J/mol D is obtained with the 0.254 [D]/[Pd] absorption point and the 0.28 [D]/[Pd] desorption point. The corresponding value for the polycrystal measurement is $\Delta\mu = 1000$ J/mol D [18]. The consistency of these numbers implies that the underlying mechanism responsible for the hysteresis, and we recognize that this mechanism is a subject of debate, is unaffected by the presence of grain boundaries in the Pd lattice.

In the absorption–desorption kinetic data presented in Fig. 2, an exponential absorption behavior was initially observed within the solid solution region that is consistent with regular lattice diffusion. The time dependence of the absorption in two-phase region was exponential as well, but characterized by a much smaller time constant, of order 200 times smaller. A similar effect has been observed by Benham and Ross [23]. These authors used a gravimetric analysis technique to record the mass uptake at constant H_2 gas pressure during absorption and desorption at 443.5 K in polycrystalline Pd foil of thickness 0.1 mm and mass 0.25 g. The mass uptake within in the two phase region was found to increase exponentially with a time constant of 0.7 l/h. This is three orders of magnitude lower than the time constant for bulk diffusion at this temperature. Given the strong temperature dependence of the Arrhenius-type phase transformation process and a sample geometry that facilitated faster transformation kinetics, our kinetic data are therefore consistent with that of Benham and Ross.

The fact that the deuteride phase transformation proceeded so slowly at the small over-pressures used in the solubility measurement had an important impact on the loading procedure of our large, bulky SANS samples. Significant over-pressures, on the order of 100 to 170 Torr

above the 65 Torr plateau pressure, were required to load the samples to the 0.031, 0.058, 0.060, and 0.097 [D]/[Pd] fraction levels. Even at these high over-pressure values, 10 to 15 h of exposure were necessary to reach the highest concentrations. On the other hand, the 0.017 [D/]/[Pd] fraction was achieved with a more modest over-pressures of 30 Torr. This loading still required 24 h to complete and was our motivation to use much higher over-pressure levels for the remaining concentration measurements.

4.2. Deuteride precipitation in single crystal pd

The observation of a Q^{-2} scattering response at high Q at the onset of precipitation can only be attributed to the formation of small deuteride plates. No other precipitation morphology can result in this single particle form factor. A plate-like morphology minimizes the lattice strain energy associated with a second phase with non-zero volume misfit [6] and is, therefore, consistent with the hypothesis that coherency and volume misfit strains are influencing initial deuteride formation. Accordingly, the observation of small plates suggests the early stages of the α' phase separation are governed by classical coherent precipitation.

The high Q data provide reliable values for the volume fraction and average plate thickness of the small deuteride plates. Our analysis demonstrates that the volume fraction remains very small, even as the deuterium loading reaches 0.06 [D]/[Pd]. The analysis also demonstrates that the average plate thickness remains small and independent of the overall deuterium loading, at least up to 0.060 [D]/[Pd]. Both of these observations suggests this component of the precipitation deuteride phase is inhibited from growth to larger volume fractions or greater plate thicknesses. It follows that the majority of deuterium precipitates into the much larger set of plates.

The Q^{-2} and Q^{-4} scattering amplitudes from Table 2 are plotted as a function of deuterium fraction in Fig. 13. The Q^{-2} response is linear over the entire deuterium fraction range probed at high Q. This, together with the approximate constant plate thickness, requires that the volume fraction of the small deuteride plates increases uniformly with deuterium loading. We interpret this as a predictable trend, not an anomaly. The Q^{-4} response is also linear of the measured concentration range. The Q^{-4} response is proportional to the interfacial surface area-to-volume ratio, as given by Eq. (2). A linear relation is expected if the particle size distribution does not change with concentration. In other words, if the large deuteride plate morphology remains constant, the total interfacial area of the deuteride phase scales with total deuterium concentration.

An optical micrograph of the 0.058 [D]/[Pd] sample surface was recorded after the sample was removed from the environmental cell. This micrograph, shown in Fig. 14, reveals the precipitation morphology of the largest deuteride particles. In our discussion of this result we first

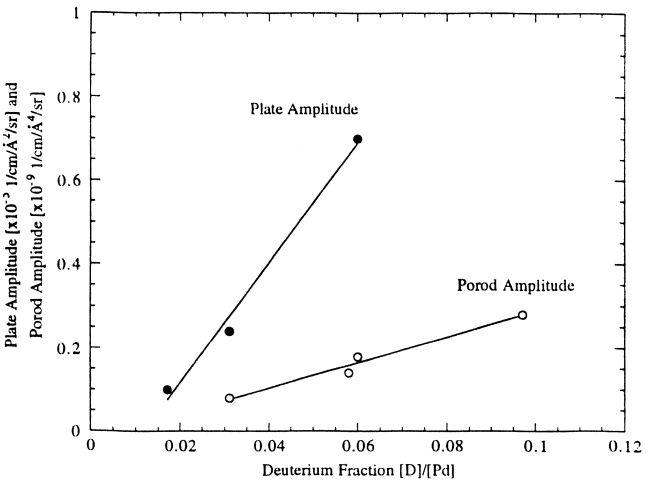

Fig. 13. A plot of the Q^{-2} (solid circles) and Q^{-4} (open circles) scattering amplitudes as a function of deuterium fraction. Both follow a linear trend over the respective composition ranges.

recount the previous TEM work of Jamieson et al. [5] and Ho et al. [24]. These authors present in situ TEM analysis of α phase nucleation during uncontrolled hydrogen desorption in α' Pd at room temperature [5] and during cooling-stage experiments [24]. Lattice damage caused by the $\alpha \rightarrow \alpha'$ transformation was avoided by loading at a temperature above the critical temperature ($T_c = 293°C$). Semi-coherent and completely incoherent plate-like α phase particles were observed on a handful of habit planes [5], consistent with our own observation of deuteride plates on the three high symmetry directions at lower deuterium fractions. The cooling experiments presented in Ref. [23] revealed the formation of coherent α-phase plates on the $\{100\}_{\alpha'}$ family of habit planes. Although coherent precipitation had been previously observed by Jamieson et al. [5], the formation on the $\{100\}_{\alpha'}$ habit plane family was new.

Ho et al. cooled their TEM specimens through the coherent solvus. The generation of elastic coherency stresses within the coherent solvus results in the formation of an array of second phase particles aligned with elastically soft host lattice directions [25,26]. This is realized to a small extend in the TEM micrographs presented by Ho et al. (see Fig. 3a in Ref. [23]). A similar constraint is also realized in Fig. 14. This figure actually reveals the remnants or scars left behind by the deuteride phase. The formation of the large plates on the $(001)_{\alpha}$ habit plane with a spacing of approximately 1 mm is evident in this figure.

The gamma-ray diffraction measurements show the effect of a broadened mosaic at high deuterium concentrations. This is certainly due to dislocation generation associated with the progression of incoherent or partially coherent phase boundaries. The gamma-ray measurements of the lower concentration sample do not indicate significant mosaic broadening. However, these data may have poor sensitivity deuteride-induced broadening due to the

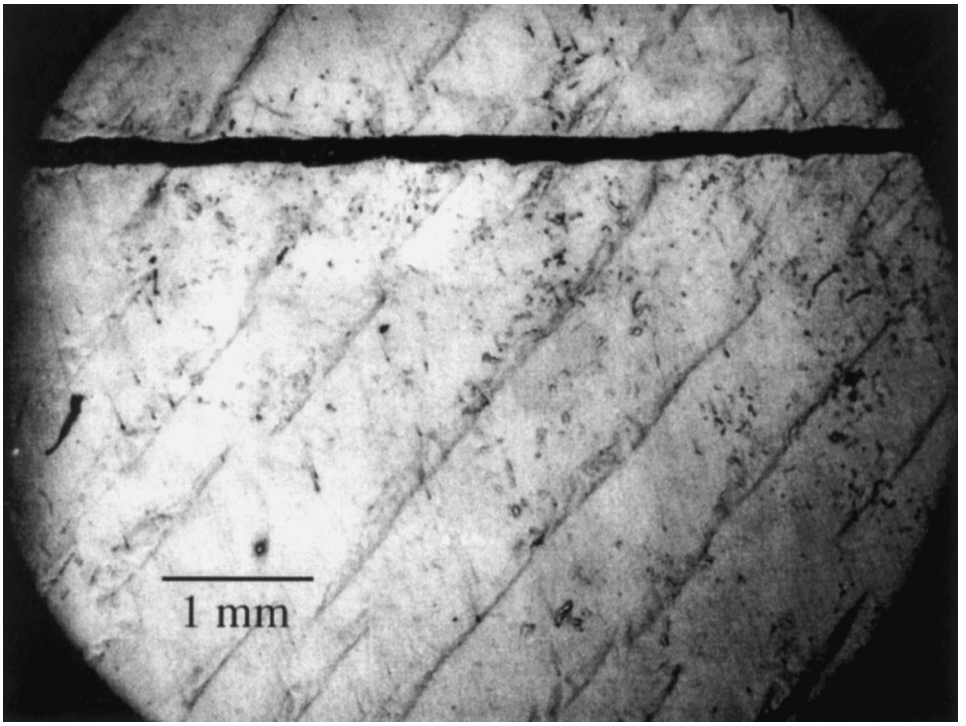

Fig. 14. Optical micrograph of the surface of the 0.058 [D]/[Pd] sample. This micrograph was recorded after the sample was removed from the environmental gas cell. The long linear features are remnants of the large deuteride plates the resulted in the anisotropic Porod response. The 3 o'clock position on this micrograph corresponds to zero sector or azimuthal angle in Figs. 8 and 9. Angles are defined in the trigonometric sense, so that the counter-clockwise direction corresponds to positive sector angles. The thick horizontal mark along the top of the micrograph is a scratch used for sample alignment.

low volume fraction of the affected lattice. Additional diffraction measurements, with an accurate determination of the relative intensity from sample to sample, are required.

5. Conclusions

In situ SANS measurements of deuteride precipitation in single crystal Pd have been presented. These measurements were complemented by a measurement of the room temperature solubility isotherm and by gamma-ray diffraction measurements. The following conclusions are based on analysis of the SANS data and the solubility measurement with the single crystal material.

1. A supersaturation of the α phase at the onset of the two phase region was observed in the single crystal material that was absent in the polycrystal isothermal measurements of some others. We believe this supersaturation is real and an inherent characteristic of the single crystal material. Supersaturation of the α phase in the single crystal material may be due to the lack of grain boundary or second phase inclusion nucleation sites.
2. The Q^{-2} scattering response observed during the precipitation process can only be attributed to the formation of small deuteride plates. The data at highest Q supported analysis of plate thickness, yielding a result of approximately 25 Å. The thickness of the small plates was found to be independent of the deuterium fraction over the range measured in this work. The volume fraction of this component of the deuteride phase was very small compared to the total volume fraction of the α′ phase based on the lever rule, except for a fraction of 0.017 [D]/[Pd] where the lever rule could not be applied. The observation of a Q^{-2} scattering response and the associated plate morphology therefore indicates that volume misfit stresses play an important role. Given the small plate thickness, particle coherency is probably maintained in the early stages of the precipitation process, consistent with classical coherent nucleation.
3. The majority of the α′ phase that formed beyond a deuterium fraction of 0.017 [D]/[Pd] was in the form of large deuteride plates favoring the $(00\bar{1})_{\alpha}$ habit plane. This conclusion is based on the correlation of the scattering anisotropy to the host lattice and visual inspection of the sample surfaces.

The formation of the deuteride phase under the conditions explored here can be outlined based on the deuteride microstructure deduced from SANS analysis. Initially, phase separation occurs by the formation of small deuteride plates consistent with classical coherent nuclea-

tion. Large pressure drives induce a coarse distribution of large, micron-thick plates in a quasi-periodic arrangement normal to the elastically-soft $[001]_{\alpha}$ direction.

Finally, we note that additional measurements are called for to further investigate deuteride formation in single crystal Pd. The present experiments involved two identical samples that exhibited very similar behavior with respect to the observed scattering response and deuteride precipitation morphology. Reproducibility has therefore been established on a limited basis. Still, these experiments were certainly influenced by the large over-pressures used for loading. Although we do not believe this invalidates our results, characterization of the precipitation process under more gradual loading conditions is appropriate.

Acknowledgements

Acknowledgment is made to the donors of The Petroleum Research Fund, administered by the ACS, for partial support of this research. We also acknowledge the support of the National Science Foundation under Grant No DMR-9496297. This research is also based upon activities supported by the National Science Foundation under Agreement No. DMR-9423101. The support of the National Institute of Standards and Technology, US Department of Commerce, in providing the facilities used in this experiment is gratefully acknowledged. The authors also acknowledge the use of 1 day of discretionary beam time granted by Dr. C. Glinka (NIST) and greatly appreciate the assistance of Dr. S. Kline (NIST). The authors also express their gratitude to Prof. T. Flanagan (Univ. Vermont) for sharing the Pd–D solubility data and to Dr. F. Ross (Univ. Missouri-Columbia) for performing the gamma-ray diffraction measurements. Finally, BJH almost missed the (premature) birth of his second son, Kyle, while away performing the NIST measurements, and would like to acknowledge the understanding of Lynn and Dale.

References

[1] P. Dantzer, in: H. Wipf (Ed.), Topics in Applied Physics, V73, Hydrogen in Metals, Vol. vol 3, Springer-Verlag, Berlin, 1997, pp. 279–331.
[2] H.K. Birnbaum, M.L. Grossbeck, M. Amano, J. Less-Common Metals 49 (1976) 357.
[3] T. Schober, Phys. Status Solidi A 29 (1975) 395.
[4] T. Schober, Phys. Status Solidi A 30 (1975) 107.
[5] H.C. Jamieson, G.C. Weatherly, F.D. Manchester, J. Less-Common Metals 50 (1976) 85.
[6] D.A. Porter, K.E. Easterling (Eds.), Phase Transformations in Metals and Alloys, 2nd ed, Chapman & Hall, London, 1992.
[7] W. Cahn, F. Larché, Acta Metall. 32 (1984) 1915.
[8] R.B. Schwarz, A.G. Khachaturyan, Phys. Rev. Lett. 74 (1995) 2523.
[9] T.B. Flanagan, J.D. Clewley, J.F. Lynch, J. Less-Common Metals 41 (1975) 343.
[10] J.F. Lynch, J.D. Clewley, T. Curran, T.B. Flanagan, J. Less-Common Metals 55 (1977) p153–163.
[11] T.B. Flanagan, B.S. Bowerman, G.E. Biehl, Scripta Metall. 14 (1980) 43.
[12] T.B. Flanagan, J.D. Clewley, J. Less-Common Metals 83 (1982) 127.
[13] B.J. Heuser, J.W. Althauser, J. Phys.: Condens. Matter 9 (1997) 8945.
[14] B.J. Heuser, J.S. King, J. Alloys Comp. 261 (1997) 225.
[15] B. Hammouda, S. Krueger, C.J. Glinka, J. Res. NIST 98 (1993) 31.
[16] T.B. Flanagan, private communication.
[17] B.J. Heuser, J.S. King, G.C. Summerfield, in: E.P. Kvam, A.H. King, M.J. Mills, T.D. Sands, V. Vitek (Eds.), Defect–Interface Interactions, (Mat. Res. Soc. Symp. Proc. Vol. 319, 1994), p. 339.
[18] T.B. Flanagan, W. Luo, J.D. Clewley, J. Less-Common Metals 172–174 (1991) 42.
[19] G. Porod, in: O. Glatter, O. Kratky (Eds.), Small Angle X-ray Scattering, Academic Press, London, 1982, pp. 17–51.
[20] M. Roth, J. Appl. Cryst. 10 (1977) 172.
[21] T.B. Flanagan, J.F. Lynch, J.D. Clewley, B. vonTurkovich, J. Less-Common Metals 49 (1976) 13.
[22] E. Wicke, J. Blaurock, J. Less-Common Metals 130 (1987) 351.
[23] M.J. Benham, D.K. Ross, Z. Phys. Chem. Neue Folge, Bd. 163 (1989) S25.
[24] E.T.C. Ho, H.A. Goldberg, G.C. Weatherly, F.D. Manchester (, in: Second International Congress on Hydrogen in Metals, 1977, pp. 1–8.
[25] J.W. Cahn, Trans. Metall. Soc. AIME 242 (1968) 166.
[26] J.W. Cahn, Acta Metall. 10 (1962) 907.